Eur Biophys J (2013) 42:683–690
DOI 10.1007/s00249-013-0918-9

ORIGINAL PAPER

EBSA
Biophysics in Europe

Effect of mutation at the interface of Trp-repressor dimeric protein: a steered molecular dynamics simulation

German Miño · Mauricio Baez · Gonzalo Gutierrez

Received: 28 December 2012 / Revised: 12 June 2013 / Accepted: 22 June 2013 / Published online: 9 July 2013

Abstract The strength of key interfacial contacts that stabilize protein–protein interactions have been studied by computer simulation. Experimentally, changes in the interface are evaluated by generating specific mutations at one or more points of the protein structure. Here, such an evaluation is performed by means of steered molecular dynamics and use of a dimeric model of tryptophan repressor and in-silico mutants as a test case. Analysis of four particular cases shows that, in principle, it is possible to distinguish between wild-type and mutant forms by examination of the total energy and force–extension profiles. In particular, detailed atomic level structural analysis indicates that specific mutations at the interface of the dimeric model (positions 19 and 39) alter interactions that appear in the wild-type form of tryptophan repressor, reducing the energy and force required to separate both subunits.

Keywords Interface stability · Dimeric proteins · Steered molecular dynamics

Introduction

Proteins are biological macromolecules with hierarchical levels of organization. Their primary structure is given by the linear polymeric sequence of amino acid residues. Their secondary structure arises from folding of the polymer, which is mainly stabilized by formation of hydrogen bonds. Tertiary structure arises as a result of interaction of segments of the secondary structure. Quaternary structure occurs when interaction causes two or more proteins to aggregate and form protein complexes which are stabilized by interfacial contact of the residues (Voet and Voet 1995). Characterization of protein–protein interactions involves identification of critical contacts that dominate the strength of the interaction (Bogan and Thorn 1998). These contacts account for most of the binding energy of the protein–protein interface. Changing these residues can disrupt stability and alter the organization of protein structure and/or the predominant state of aggregation (Rumfeldt et al. 2008). Experimentally, high-energy residues at an interface are evaluated by generating point mutations that modify the chemical nature of a specific contact, i.e., an apolar residue is replaced by a polar one or a bulky residue is replaced by a small residue. Thus, prediction of the possible result of mutations of interfacial contacts would be highly desirable. Here we report results from analysis of changes in the force and energy required to separate, along a predefined reaction coordinate, mutant forms of the Trp-repressor compared with the native form.

Several theoretical methods for evaluation of the effect of mutations in protein interactions can be found in the literature (Carra et al. 2012; Gao et al. 2004; Kamisetty et al. 2011). Here we investigate a different method based on steered molecular dynamics (SMD) simulation. SMD simulation is a theoretical technique that enables investigation of biological processes on time scales accessible to molecular level simulations, for example unbinding of ligands and conformational changes in biomolecules (Balsera et al. 1997; Deulfhard et al. 1998). The effects of

G. Miño (✉) · G. Gutierrez
Group of NanoMaterials, Departamento de Física, Facultad de Ciencias, Universidad de Chile, Casilla 653, Santiago, Chile
e-mail: germino@u.uchile.cl

M. Baez
Laboratorio de Bioquímica, Facultad de Ciencias Químicas y Farmacéuticas, Universidad de Chile, Santos Dumont No. 964, Santiago, Chile

mutations are evaluated by computing total energy and force–extension profiles of the process of contact rupture during molecular stretching. Similar evaluations using force–extension profiles obtained by SMD can be found in the literature (Bayas et al. 2004; Shen et al. 2012) These studies involve manipulation of single proteins by use of optical tweezers or atomic force microscopy (Shank et al. 2010; Alessandrini and Facci 2005). In these techniques the protein is stretched along a unique reaction coordinate and the force and energy determined are representative of the structural or mechanical stability along this coordinate (Li et al. 2000; Best et al. 2008). The tryptophan repressor (Trp-repressor, pdb-id:3wrp) was chosen as a study model. Trp-repressor is a symmetrical homodimeric DNA-binding protein of 108 amino acids per subunit that regulates the synthesis of tryptophan (Zhang et al. 1987). Trp-repressor has an all-α-helix architecture. Each subunit consists of 6 intertwining helices (Fig. 1) in the folded complex. Three α-helices (A–B–C) of each subunit compose the core domain and the interface of the dimeric complex, and the other three α-helices (F–E–D) of each subunit form the DNA binding domains. Experimental studies have revealed that two key positions at the interface are important for its stabilization. These are tryptophan 19 (W19) and leucine 39 (L39) that are part of the A and B α-helices, respectively. Note that as the dimer is symmetrical, they appear in both subunits. Site-specific mutation of wild type (WT) W19 for phenylalanine (F) has been reported to induce disruption of the dimer interface (Royer et al. 1993). Also, mutation of WT L39 for glutamic acid (E) destabilizes the interaction at the dimer interface and enables a monomeric form of Trp-repressor to occur (Shao et al. 1997). In the latter case the mutation increases the dissociation constant from 1 nM to 0.11 mM (Mann and Matthews 1993; Shao et al. 1997). Our molecular level simulations of four particular cases show that it is possible, in principle, to distinguish between WT and mutant forms by examining total energy and force–extension profiles, where higher energy and forces are required to separate the subunits of the WT form. Visualization of the molecular events along the SMD extension is also analyzed, and a cogent rationale of the forces required for subunit dissociation is given.

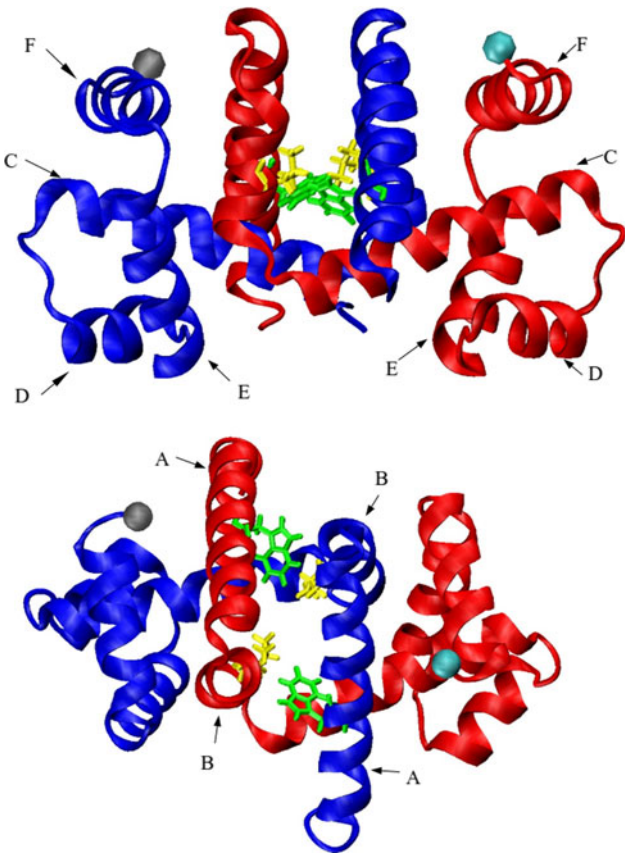

Fig. 1 Frontal and superior view of the TR model showing both subunits (*blue* and *red*), residues W19 (*green*) and L39 (*yellow*), fixed SMD atom (*gray*), and mobile SMD atom (*cyan*)

Methods and computational details

The main technique used in this work is molecular dynamics (MD) simulation. In the MD approach, the phase space trajectories of the system (positions and velocities of all atoms at all times) are obtained by numerical resolution of the equation of motion of the whole system. Thus, atoms (or molecules) are treated as classical particles that obey Newton's equations of motion. A crucial step is selection of force fields that can be obtained by means of empirical potentials (the so-called "classical MD") or by means of quantum mechanical calculations, via the Hellman–Feynman theorem ("ab initio" or "first principles MD") (Gutierrez et al. 2010). In the SMD method an external force is applied to an atom (or group of atoms), the so-called SMD atom, along a reaction path. The SMD atom is attached to a dummy atom via a virtual spring while a reference atom (or group of atoms) is kept fixed. The dummy atom can then be moved at constant velocity along the reaction coordinate, dragging the SMD atom. In our case, the force $\vec{F}$ between the dummy and SMD atoms is determined from the potential energy, U, by using

$$\vec{F} = -\nabla U, \quad \text{with} \quad U = \frac{1}{2}k[vt - (\vec{r} - \vec{r}_0) \cdot \vec{n}]^2,$$

where k is the spring constant, v is the pulling velocity, t is time, $\vec{r}$ is the position of the SMD atom during the extension procedure, $\vec{r}_0$ is the initial position of the SMD atom, and $\vec{n}$ is the direction of pulling. In this way, it is possible to measure the energy and force required to separate a ligand from its binding site or to extend or unfold a biopolymer.

The SMD simulations were performed on the WT form of Trp-repressor and on the mutant forms W19F and L39E. As the protein model is a homodimer, both subunits were mutated. The nomenclature for these three homodimeric models is WT/WT, W19F/W19F, and L39E/L39E, respectively. A third mutant form was designed by using one WT subunit and one W19F mutant subunit. This heterodimeric model is named W19F/WT. Each structure was embedded in a sphere of 3520 TIP3 water molecules, padding sufficient to cover the dimeric model in each case. The carbon atoms α to aspartate 108 of each opposite subunit were chosen as the fixed and mobile (SMD) atoms (Fig. 1). The subunit to which the fixed (or mobile) atom belongs is referred to as fixed (or mobile) subunit throughout the text. The fixed SMD atom distance is used as a control variable for the SMD simulations. All the simulations were performed by use of NAMD2.7 software (Kale et al. 1999) using the CHARMM22 potential with CMAP correction (MacKerell et al. 1998). The structures were minimized over 10^5 steps and further equilibrated at 310 K for 1 ns at constant temperature by use of Langevin dynamics with a damping coefficient $\gamma = 5\ \mathrm{ps}^{-1}$. An integration time step of 1 fs was used with a uniform dielectric constant of 1 and a cutoff of non-bonded forces with a switching function starting at a distance of 10 Å and reaching zero at 13.5 Å (Lu and Schulten 1999). The SMD simulations were performed at a constant velocity of $0.0005\ \text{Å/fs} = 50\ \text{m/s}$ with a $7\ \text{kcal/mol/Å}^2$ spring constant. No thermal constraints were applied during the SMD procedure. Visualization and data analysis were performed by use of VMD 1.8.7 software (Humphrey et al. 1996).

Results

The trajectory of SMD simulation at 40, 130, 430, 470, and 680 Å of extension between the fixed and SMD atoms is shown in Fig. 2 for the WT/WT form. Between 40 and 430 Å of extension, α-helices C, D, E, and F of both subunits undergo simultaneous unfolding without significant changes of the core domain. From 430 to 470 Å the core domain partially unfolds keeping the contacts between helical structures A–B–C nearly constant. Further extension, from 470 to 680 Å, disrupts these contacts and the α-helical structure of helices A and B is gradually lost until the subunits are completely detached. A similar structural response is observed for the other three mutants as the SMD simulation is performed.

The energy profile calculated from the SMD trajectories is shown in Fig. 2, lower panel. For all the proteins, three main events can be distinguished. First, between 100 and 200 Å, a smooth change in the slope is indicative of symmetrical unfolding of the external domain (D–E–F) of both subunits. Next, a second increase in the slope, from 430 to 470 Å, is indicative of partial distortion of the core

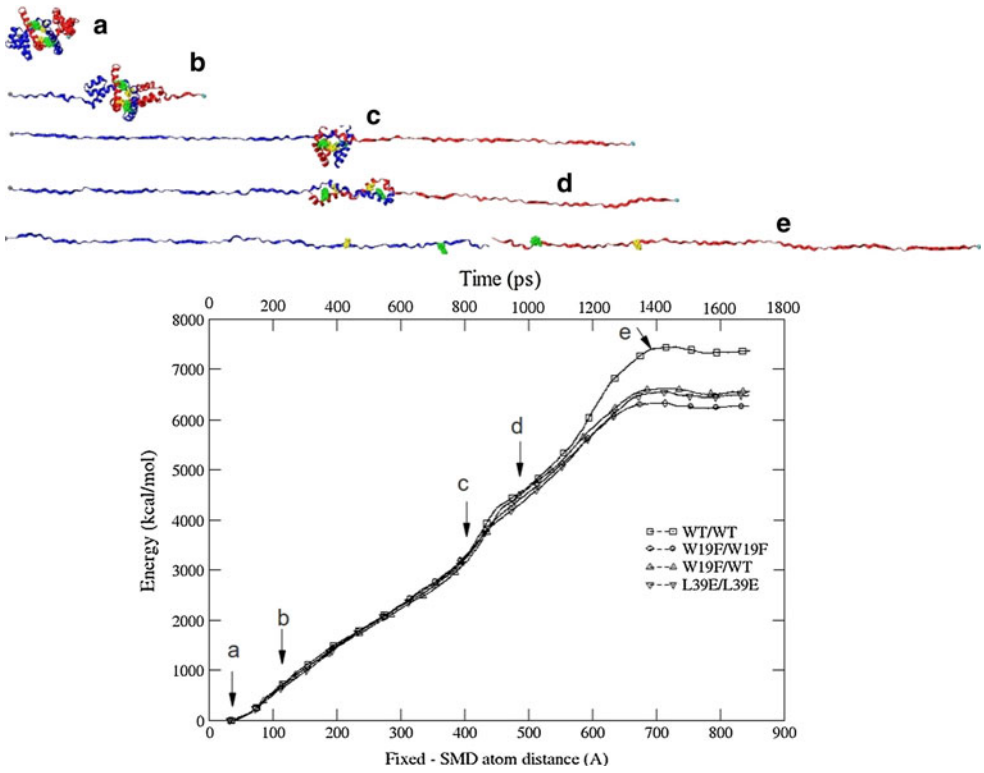

Fig. 2 Evolution of the SMD simulation for the WT/WT form. *Upper panel* snapshots at **a** 40 ($t = 0$), **b** 130, **c** 430, **d** 470, **e** 680 Å between the fixed and SMD atoms. Residues W19 (*green*) and L39 (*yellow*) in each subunit are depicted as references. *Lower panel* energy profiles along the extension coordinate for WT/WT, W19F/W19F, W19F/WT, and L39E/L39E forms. *Letters* with *arrows* refer to the snapshots in the *upper panel*

without major change of the interfacial contacts between the AB segments of each subunit. The final event is a plateau associated with the complete unfolding and detachment of these segments. At this plateau the analyzed cases follow the decreasing energetic order: WT/WT > W19F/WT > L39E/L39E > W19F/W19F. In this last event, the WT/WT form requires more energy, which is reflected in its resistance to dissociation. This resistance is reflected in the greater area under the curve. The mutant form W19F/W19F has the lowest resistance to subunit separation. An intermediate response was observed for the forms L39E/L39E and W19F/WT. This initial energy profile shows the response of the models is in agreement with the experimental outcomes, in the sense that the interfacial contacts of the WT/WT form are more stable than those of the mutant forms W19F/W19F and L39E/L39E. Although only four cases were analyzed, our results suggest more energy is needed to unfold the WT/WT form at approximately 600 Å. This suggests that W19 and L39 are of crucial importance to the structural stability of the dimer.

Further insight into this process can be obtained by examining the force (pN) versus extension plots of the SMD procedure, shown in Fig. 3. In general, each of the four force–extension profiles contains two regions where the force is maximum, one at approximately 440 Å and the other at 570 Å. The first main peak (440 Å) involves unfolding of the C–D–E–F α-helices together with partial distortion of the helices that comprise the dimer interface. The second main peak (570 Å) is related to unfolding and dissociation of Trp-repressor. Comparison of the four different force–extension profiles reveals that dimers WT/WT and W19F/WT have the highest first main peaks of the set, that of WT/WT being broader than that of W19F/WT. Considering that the area below the curve in the force–extension profiles corresponds to the amount of energy required to unfold the system, its evaluation gives us an estimate of the flexibility of the structure. For the two mutants W19F/W19F and L39E/L39E, the first peak is sharper and lower, indicating increased structural flexibility of their core domain. In the same way, the flexibility of heterodimer W19F/WT is between that of the WT/WT and W19F/W19F forms. The main difference between the WT/WT form and the mutants is in the region that involves separation of the subunits, that is, from 490 to 680 Å. This peak is highest for the WT/WT protein, approximately 1,500 pN; in the mutant forms the second peak is clearly diminished and divided into several small peaks that reach 1,000 pN.

Detailed analysis of residue–residue distance versus fixed SMD atom distance at lengths ranging from 490 to

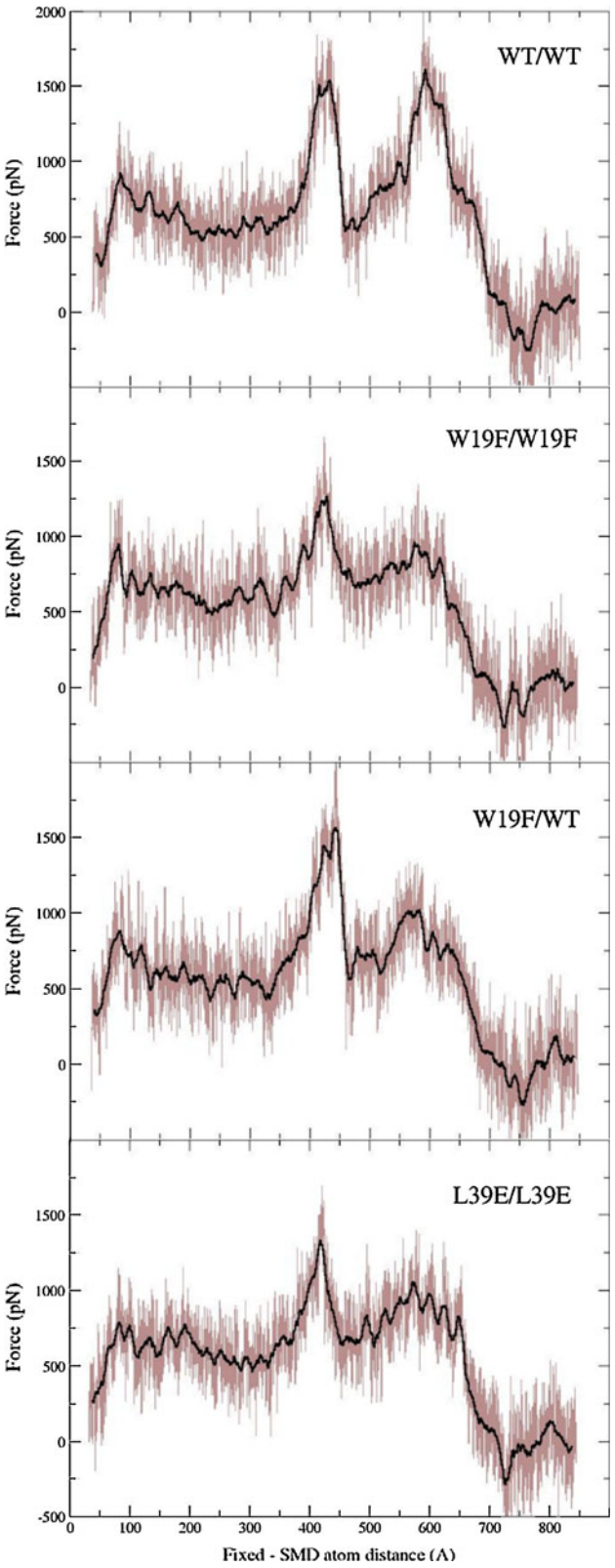

Fig. 3 Force–extension profiles for the WT/WT, W19F/W19F, W19F/WT, and L39E/L39E forms of the Trp-repressor

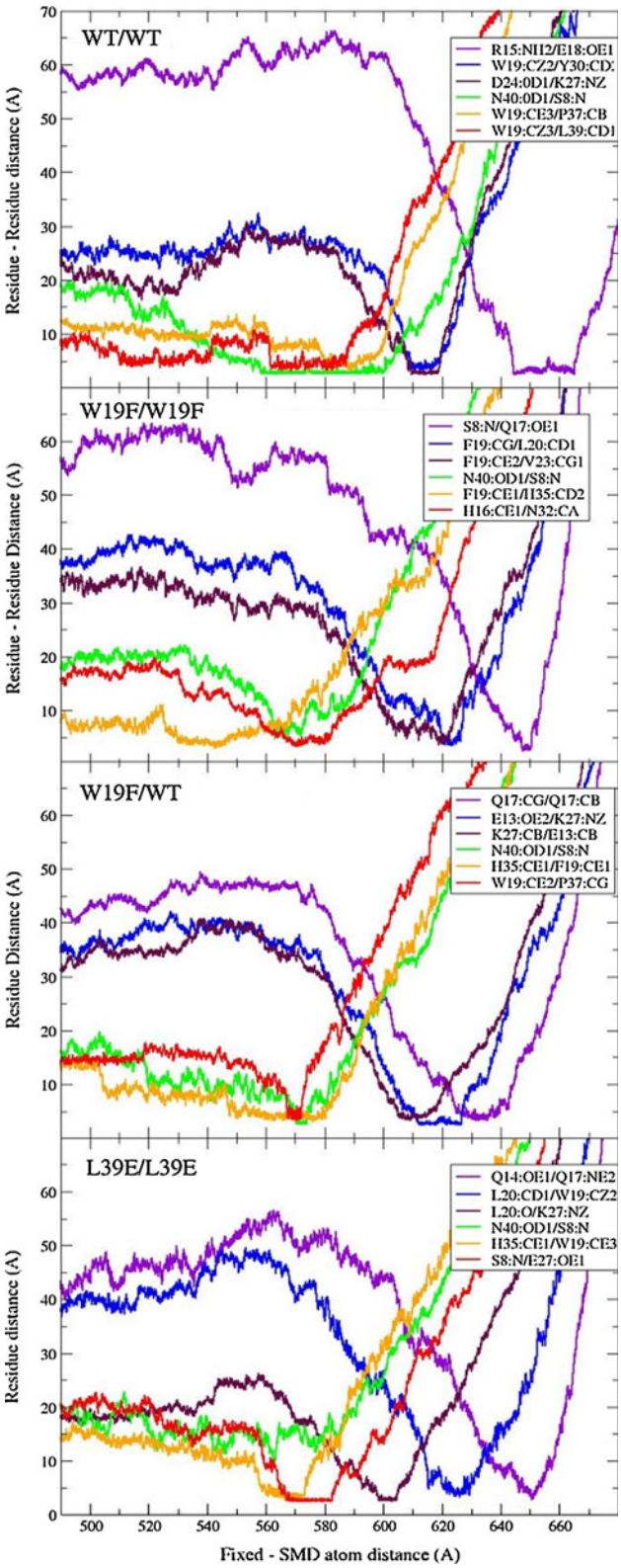

◀ **Fig. 4** Relevant contacts from 490 to 680 Å for the WT/WT, W19F/W19F, W19F/WT, and L39E/L39E forms of the Trp-repressor. The measured distance involves two atoms of each pair of residues. These atoms are labeled in accordance with the nomenclature of the top_all27_prot_lipid.inp file available at http://www.ks.uiuc.edu/Research/vmd/plugins/membrane/top_all27_prot_lipid.inp

680 Å is particularly revealing of the profile of the second peak. Figure 4 shows this analysis in this range for all cases. The criterion for contact formation was a residue–residue distance <3.8 Å. In general, polar–polar contacts seem brittle and sharp, that is, they form and break discontinuously. On the other hand, apolar–apolar contacts change smoothly as they appear. Both kinds of contact reinforce each other, giving rise to the peak shapes. For these analyses we used the one-letter nomenclature for the residues and used the slash (/) to represent an interaction. For example, N40/S8, represents the interaction between Asparagine 40 (located in the fixed subunit) and Serine 8 (located in the mobile subunit). For WT/WT the polar contact between N40 and S8 seems to be correlated with the maximum value observed for the second peak. This interaction starts at 560 Å and disappears at 600 Å, exactly when the maximum value of the second peak is observed. Other polar contacts, for example D24/K27 and R15/E18, seem to give the shoulders at approximately 615 and 655 Å, respectively. Other non-polar contacts, for example W19/Y30, W19/P37, and W19/L39 form along the second peak. For W19F/W19F a different set of contacts is correlated with the shape of the second main peak. Here the maximum value is approximately 577 Å, which correlates with the H16/N32 contact. After that, a small peak appears at 618 Å, which correlates with the F19/V23 and F19/L20 contacts. A shoulder is observed at 645 Å and correlates with the S8/Q17 contact. N40/S8 is not relevant role in generation of resistance to separation of the two subunits, as observed in the WT/WT case. For the W19F/WT case, the maximum value is at approximately 560–590 Å, which correlates with the H35/F19, H16/N32, and N40/S8 contacts. A small peak then appears at 605 Å, which correlates with the K27/E13 contact. A smaller peak is observed at 630 Å and is correlated with the Q17/Q17 contact. Again, the N40/S8 contact is not relevant in generation of resistance to separation of the two subunits. For L39E/L39E, a clear correlation is established for the four small peaks with a saw-tooth shape that are observed between 570 and 650 Å (Fig. 3). The first, at 570 Å, is correlated with the H35/W19 contact. The second, at 600 Å, is correlated with L20/K27. The third, at 625 Å, is correlated with L20/W19 and the fourth, at 650 Å, is correlated with Q14/Q17. Again, the N40/S8 contact seems to be irrelevant.

Because the mutations involved positions 19 and 39, detailed investigation of the molecular events associated with these particular residues was conducted in the 520–610 Å distance ranges. This range involves the second main peak for all forms. Inspection of the WT/WT form shows that both W19 and L39 interact alternately with P37

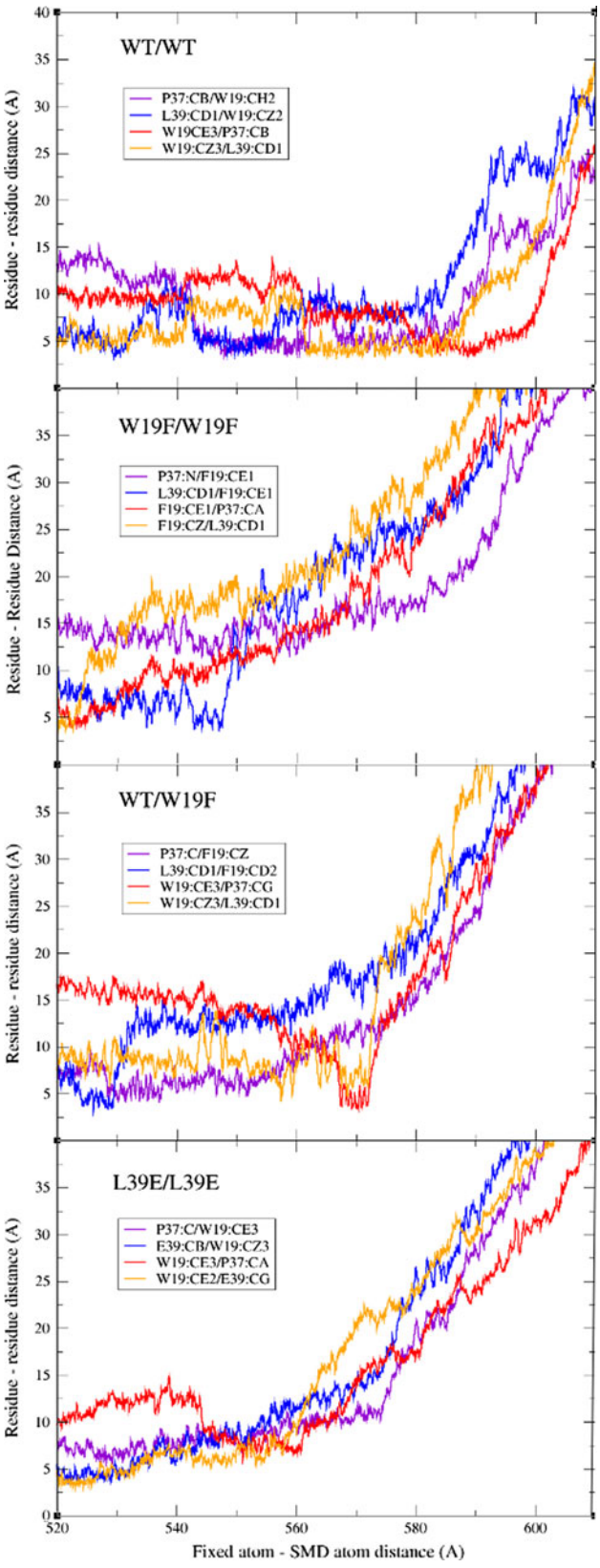

◀ **Fig. 5** Relevant residue–residue distances for the WT/WT, 19F/W19F, W19F/WT, and L39E/L39E forms of the Trp-repressor. The measured distances involve two atoms of each pair of residues. These atoms are labeled in accordance with the nomenclature of the top_all27_prot_lipid.inp file available at http://www.ks.uiuc.edu/Research/vmd/plugins/membrane/top_all27_prot_lipid.inp

(Fig. 5, WT/WT case). Because of the symmetry of the dimeric model, the W19–P37–E39 interaction seems doubled between 520 and 590 Å. The first event is alternate interaction of P37 and L39 of the mobile subunit with W19 of the fixed subunit. For WT/WT these interactions are represented by the blue (L39–W19 interaction) and violet (P37–W19 interaction) curves of Fig. 5. Initially L39–W19 briefly interacts at 530 Å, then the interaction is recovered at 542 Å continuing until 555 Å. Meanwhile, the P37–W19 interaction starts at 542 Å, experiences an interval from 562 Å, and is recovered at 568 Å and continues until 585 Å. The second symmetrical interaction in the WT/WT model occurs between W19 of the mobile subunit and L39 and P37 of the fixed subunit. For WT/WT its evolution is shown by the orange (W19–L39 interaction) and red (W19–P37 interaction) curves of Fig. 5. Here, W19–L39 interacts from 510 to 590 Å, with an interval between 530 and 560 Å. Around 585 Å exchange of W19 between L39 and P37 occurs, and the W19–P37 interaction starts and continues until 590 Å. For WT/WT these interactions are shown as molecular events in Fig. 6. Interestingly, for both of these symmetrical interactions, W19–P37–L39 point toward a common center when formed. The occurrence of these two interactions seems to be correlated with the appearance of the second peak, as is suggested from analysis of the corresponding interactions in the mutant forms. For W19F/W19F relevant interactions are those of L39/F19 and F19/L39, which symmetrically appear as the polypeptide chains are stretched (blue and orange curves of Fig. 5 for W19F/W19F). Here P37 does not interact either with F19 or L39 (red and violet curvesin Fig. 5 for W19F/W19F). The molecular arrangement of L39, F19, and P37 associated with these events is shown in Fig. 6 for W19F/W19F. It is apparent the F19–L39 residues point toward a common position; nevertheless P37, on both sides, does not interact with either of these two residues. The smaller size of F compared with W probably prevents formation of the stabilizing interactions observed for WT/WT. For the W19F/WT mutant the analysis can be performed by combining the considerations for the WT/WT and W19F/W19F forms. Here only one of the two symmetrical interactions arises, W19–P37–L39; the second interaction, F19–P37–L39, is not observed. The former appears at 566 Å (red and orange curves of Fig. 5 for W19F/WT) whereas significant interaction of F19–L39 is observed for the latter only, at 528 Å (blue and violet curves of Fig. 5 for W19F/WT). The molecular snapshots for this case are depicted in Fig. 6 for W19F/WT. Here, the arrangement of residues W19–P37–L39 is similar to that observed for WT/WT, with all three pointing toward a common center.

For the F19–P37–L39 residues only the interaction between F19–L39 is detected. Nevertheless P37 points in the other direction, as observed for W19F/W19F. For the last mutant, L39E/L39E, an interaction is found for W19–E39 only; again P37 does not participate in any interaction. As can be seen in Fig. 5 the two relevant symmetrical interactions appear, namely, E39/W19 (blue curve) and W19/E39 (orange curve) on either side. Those interactions persist until 530 Å. The snapshots for this case, Fig. 6 L39E/L39E, show that E39 partially interacts with W19, through the β or γ carbon, and that the P37 are, as for the previous mutants, oriented away from any common point. These results suggest that the WT/WT interactions, namely W19–P37–L39, give rise to the second peak observed for the force–extension profiles and the introduced mutations reduce the intensity of this peak.

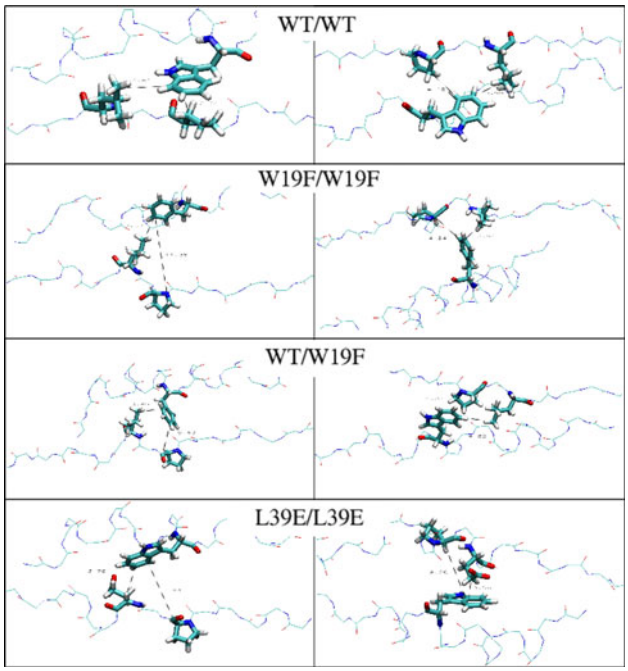

Fig. 6 Molecular snapshots for the 19–37–39 residues. From *top* to *bottom* WT/WT form, (*left*) first transient interaction, at 554 Å, formed between the P37 and L39 residues of the mobile subunit and the W19 residue of the fixed subunit (*violet* and *blue* curves of Fig. 5 for WT/WT); (*right*) second transient interaction, at 585 Å, formed between residue W19 of the mobile subunit and residues L39 and P37 of the fixed subunit (*red* and *orange* curves of Fig. 5 for WT/WT). W19F/W19F form, (*left*) interaction at 546 Å between F19 in the mobile subunit and L39 in the fixed subunit (*blue* curve in Fig. 5 for W19F/W19F); (*right*) interaction at 522 Å between L39 in the mobile subunit and F19 in the fixed subunit (*orange* curve in Fig. 5 for W19F/W19F). W19F/WT form, (*left*) interaction at 528 Å between F19 in the mobile subunit and L39 in the fixed subunit (*blue* curve in Fig. 5 for W19F/WT); (*right*) interaction at 566 Å between P37 and L39 both located in the mobile subunit and W19 located in the fixed subunit (*red* and *orange* curves of Fig. 5 for W19F/WT). L39E/L39E form, (*left*) interaction at 521 Å between W19 located in the mobile subunit and E39 located in the fixed subunit (*blue* curve in Fig. 5 for L39E/L39E); (*right*) interaction at 514 Å of extension, between E39 located in the fixed subunit and W19 in the mobile subunit (*orange* curve of Fig. 5 for L39E/L39E)

Discussion and conclusions

Our results show it is possible to perform a coherent study of the effects of mutations on the structural stability of interfaces by following the total energy required to separate the two subunits. The important regions of the interface of the Trp-repressor dimer have been evaluated by introducing point mutations (Royer et al. 1993; Shao et al. 1997). The mutational changes W19F and L39E result in dissociation of the dimer at lower protein concentrations. For L39E, the dissociation constant changes from 1 nM to 0.11 mM (Shao et al. 1997).

Force–extension profiles show that a structurally stable interface requires greater force to achieve subunit separation. Also, the SMD method enables analysis of molecular details associated with subunit separation. In the Trp model, the main source of structural stability seems to be interaction of the W19–P37–L39 residues that appear symmetrically in both subunits. In WT/WT, as the SMD simulation evolves, these three residues form a transient cluster that correlates with the peak at approximately 600 Å. Analysis of molecular events shows that these residues point toward a common center when they make contact. Exchanging tryptophan for a smaller residue, in W19F/W19F, seems to reduce the probability of contact between these three positions. Here a change of a bulky residue, W, for a smaller one, F, at position 19 seems to reduce the possibility of contact between positions 19, 37, and 39. In this work, visualization of the molecular events revealed interaction between W19 and L39. Nevertheless both prolines (P37) point away, preventing formation of the clusters. This spatial arrangement is consistently observed on both sides of the symmetrical detachment of the fixed and mobile subunits. For mutant W19F/WT, events associated with the W19–P37–L39 and F19–P37–L39 interactions can be interpreted as a combination of the two previous cases. Graphical depiction of the molecular events shows that in the former group of residues, the transient cluster is formed and they do point to a common center as occurs for WT/WT. For the latter group of residues this clustering does not occur in a similar way to that in the mutant W19F/W19F. For the last case, L39E/L39E, exchanging L39 for a charged group, E, again prevents formation of clusters and the interaction of W19–E39 occurs through the γ or δ carbon of E39, and P37 residues evolve pointing outwards. This situation is consistently replicated on both sides of the subunit separation for the L39E/L39E mutant form. Overall, the results suggest that the reduction of the second peak at approximately 600 Å

correlates with mutational changes of the residues at positions 19 and 39.

In conclusion, in this work we present an analysis of events in the process of symmetrical dissociation of dimeric models of Trp-repressor. Our simulations in four cases reveal that introduction of mutations at the interface substantially reduce the structural stability of the surface connecting the subunits. The change in structural stability can be readily followed by energy considerations and by force–extension profiles involved in the SMD procedure. In particular, on the basis of results we conclude that for mutations W19F and L39E the energy at the interface and the force required to separate the dimer are both lower, reducing the structural stability of the system. Analysis of the molecular events is also useful for understanding and explaining the changes observed in mutants. For instance, in single-molecule experiments using optical tweezers or atomic force microscopy (Shank et al. 2010; Alessandrini and Facci 2005) the protein is unfolded by traction at fixed points of the polypeptide and the same unfolding coordinate can subsequently be investigated. This enables measurement of the magnitude of the forces involved in protein secondary and tertiary structure. In the same way, our research investigated the structural stability of interfaces of the dimeric Trp-repressor and its mutants, and we showed it is possible, in principle, to evaluate subtle changes in stability by changes in the key residues that are parts of these interfaces.

Acknowledgments The authors gratefully thank Fondo Nacional de Desarrollo Científico y Tecnologíco, Fondecyt Grants no. 3110149 (GM), 11110534 (MB). GG acknowledges partial support of Fondecyt-Chile 1120603. This work have also been supported by the High-Performance Computing infrastructure of the Center for Mathematical Modeling, University of Chile, via the Project BASAL-CMM. The authors warmly thank Professors Boris Weiss-López and Bruce Kennedy Cassels for their useful insight and for critical reading of the manuscript.

References

Alessandrini A, Facci P (2005) AFM: a versatile tool in biophysics. Meas Sci Technol 16:R65–R92

Balsera M, Stepaniants S, Izrailev S, Oono Y, Schulten K (1997) Reconstructing potential energy functions from simulated force-induced unbinding Processes. Biophys J 73:1281–1287

Bayas M, Schulten K, Leckband D (2004) Forced dissociation of the strand dimer interface between C-cadherin ectodomains. Mech Chem Biosyst 1:101–111

Best R, Paci E, Hummer G, Dudko O (2008) Pulling direction as a reaction coordinate for the mechanical unfolding of single. J Phys Chem B 112:5968–5976

Bogan AS, Thorn KS (1998) Anatomy of Hot spots in protein interfaces. J Mol Biol 1:1–9

Carra C, Saha J, Cucinotta FA (2012) Theoretical prediction of the binding free energy for mutants of replication protein A. J Mol Model 18:3035–3049

Deulfhard P, Hermans J, Leimkuhler B, Mark AE, Reich S, Skeel RD (eds) (1998) computational molecular dynamics: challenges, methods, ideas, vol 4. Lecture Notes in Computational Science and Engineering. Springer, Berlin

Gao Y, Wang R, Lai L (2004) Structure-based method for analyzing protein–protein interfaces. J Mol Model 10:44–54

Gutierrez G, Menendez-Proupin E, Loyola C, Peralta J, Davis S (2010) Computer simulation study of amorphous compounds: structural and vibrational properties. J Mater Sci 45:5124–5134

Humphrey W, Dalke A, Schulten K (1996) VMD—visual molecular dynamics. J Mol Graph 14:33–38

Kale L, Skeel R, Bhandarkar M, Brunner R, Gursoy A, Krawetz N, Phillips J, Shinozaki A, Varadarajan K, Schulten K (1999) NAMD2: greater scalability for parallel molecular dynamics. J Comp Phys 151:283–312

Kamisetty H, Ramanathan A, Bailey-Kellogg C, Langmead CJ (2011) Accounting for conformational entropy in predicting binding free energies of protein–protein interactions. Proteins 79:444–462

Li H, Oberhauser A, Fowler S, Clarke J, Fernandez J (2000) Atomic force microscopy reveals the mechanical design of a modular protein. PNAS 97:6527–6531

Lu H, Schulten K (1999) Steered molecular dynamics simulations of force-induced protein domain unfolding. Proteins Struct Funct Genet 35:453–463

MacKerell AD Jr, Bashford D, Bellott M, Dunbrack RL Jr, Evanseck J, Field MJ, Fischer S, Gao J, Guo H, Ha S, Joseph D, Kuchnir L, Kuczera K, Lau FTK, Mattos C, Michnick S, Ngo T, Nguyen DT, Prodhom B, Reiher IWE, Roux B, Schlenkrich M, Smith J, Stote R, Straub J, Watanabe M, Wiorkiewicz-Kuczera J, Yin D, Karplus M (1998) All-atom empirical potential for molecular modeling and dynamics studies of proteins. J Phys Chem B 102:3586–3616

Mann C, Matthews CR (1993) Structure and stability of an early folding intermediate of *Escherichia coli* trp aporepressor measured by far-uv stopped-flow circular-dichroism and 8-anilino-1-naphthalene sulfonate binding. Biochem 32:5282–5290

Royer CA, Mann CJ, Matthews CR (1993) Resolution of the fluorescence equilibrium unfolding profile of trp aporepressor using single tryptophan mutants. Protein Sci 2:1844–1852

Rumfeldt JAO, Galvagnion C, Vassall KA, Meiering EM (2008) Conformational stability and folding mechanisms of dimeric proteins. Prog Biophys Mol Biol 98:61–84

Shank E, Cecconi C, Dill J, Marqusee S, Bustamante C (2010) The folding cooperativity of a protein is controlled by its chain topology. Nature 465:637–640

Shao X, Hensley P, Matthews CR (1997) Construction and characterization of monomeric tryptophan repressor: a model for an early intermediate in the folding of a dimeric protein. Biochem 36:9941–9949

Shen M, Guan J, Xu L, Yu Y, He J, Jones GW, Song Y (2012) Steered molecular dynamics simulations on the binding of the appendant structure and helix-β2 in domain-swapped human cystation C dimer. J Biomol Struct Dyn 30:652–661

Voet D, Voet J (1995) Biochemistry, 2nd edn. Wiley, New York

Zhang RG, Joachimiak A, Lawson CL, Schevitz RW, Otwinowski Z, Sigler PB (1987) The crystal structure of trp aporepressor at 1.8 Å shows how binding tryptophan enhances DNA affinity. Nature 327:591–597